ORIGINAL PAPER

Mechanochemical synthesis and electrochemical properties of nanostructured electrode materials for Li ion batteries

G. Mulas · S. Enzo · C. Bonatto Minella · E. Arca ·
C. Gerbaldi · N. Penazzi · S. Bodoardo · J. Hassoun ·
S. Panero

Abstract We focus on the synthesis by ball milling and on the electrochemical characterization of nanocrystalline bimetallic and composite materials to be employed as anodes in Li ion batteries. Ni_3Sn_4 and Ni_3Sn_2 based compounds were obtained by ball milling of three different Ni–Sn mixtures. The properties of the resulting anodes for Li ion batteries were evaluated as a function of composition. Moreover, a biphasic system is presented, with $CoSn_2$ and $CoSn$ type structures, arising from the synthesis of the $Sn_{31}Co_{28}C_{41}$ composition. When cycled in a Li cell, this material showed a high reversible specific capacity, about 450 mA h g^{-1}, and a very good electrochemical and structural stability, making it of interest for application purposes.

Keywords Nanostructured materials · Ball milling ·
Li ion batteries · Kinetics

G. Mulas (✉) · S. Enzo · C. Bonatto Minella · E. Arca
Dipartimento di Chimica, Università di Sassari,
Via Vienna 2,
I-07100 Sassari, Italy
e-mail: mulas@uniss.it

C. Gerbaldi · N. Penazzi · S. Bodoardo
Dipartimento di Scienza dei Materiali ed Ingegneria Chimica,
C.so Duca Abruzzi 24, Politecnico di Torino,
I-10129 Turin, Italy

J. Hassoun · S. Panero
Dipartimento di Chimica,
Università di Roma "La Sapienza", P.le Aldo Moro 5,
I-00185 Rome, Italy

Introduction

The development of advanced materials for energy storage and conversion has been receiving wide attention to meet the rising demand of clean energy technologies. In particular, a large effort is being devoted towards the improvement of the specific properties of electrochemical devices such as rechargeable lithium ion batteries, through the investigation of nanostructured bi- or multicomponent alloys for electrodes [1–6]. Besides the enhanced electrochemical reactivity related to the thermodynamic metastability, the structural features of nanocrystals could offer several advantages with respect to the fully crystalline counterparts as, for instance, short path length for electronic and cation transport, higher electrode active specific area, which can result in higher capacity and significant rate capability [1–3].

Mechanochemical synthesis by ball milling is recognised to be a powerful technique for the preparation of a variety of metastable materials including nanostructured as well as amorphous and quasicrystalline phases [7, 8]. The relative simplicity and cheapness of the technique, together with its flexibility, has stimulated recent and rising attention by the scientific community for the preparation of nanostructured materials for power sources technologies [9–12].

Along this line, in this contribution we focus on the synthesis by mechanical processing and on the electrochemical properties of nanocrystalline tin-based alloys, which were studied as Li ion battery anode materials. An overview of more recent results of the authors is here presented, while the relevant extended discussion is reported in the cited references [13–15]. The interest in the Sn-based systems [16, 17] is related to the electrochemical properties arising from the coupling of the specific role of Sn phase, active in the Li ion intercalation

process with the buffering role of transition metals, able to assist the volume expansion during the lithiation. As a matter of fact, in Sn-based materials, the expected reversible electrode process is illustrated by the reaction:

$$Sn + 4.4Li^+ + 4.4e^- \leftrightarrow Li_{4.4}Sn \qquad (1)$$
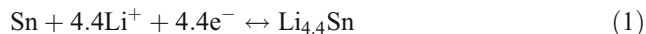
to which a theoretical specific capacity of 993 mA h g^{-1} is associated [18]. Depending on the electrode's stoichiometry, their theoretical specific capacity can be evaluated [13, 14, 16, 19]. Thus, Ni and Co were selected as metals inactive against Li. Through a detailed structural and thermodynamic investigation, we attempted to optimise the microstructural features to improve the electrochemical performance.

Materials and methods

Elemental powders (99.9% purity at least) purchased from different commercial sources were used as starting materials. The mechanical treatments were carried out by ball milling using a SPEX Mixer-Mill Model 8000 equipped with stainless-steel vial and spheres. The vial was charged with 8 g powder and two balls whose mass was properly selected to vary the impact energy conditions. To avoid gaseous contamination, vial charging and sampling were performed in an Argon-filled MBraun glove box, which maintained oxygen, moisture and nitrogen content below 2 ppm.

The structural evolution of solid phases was investigated by X-Ray Diffraction (XRD), performed in step scanning mode by a Rigaku DMax diffractometer equipped with Cu-Kα radiation and graphite monochromator in the diffracted beam. Microstructural features and phase abundance were quantitatively evaluated by integral inversion routines according to the Rietveld method [20]. The thermal stability of the powders was evaluated by Differential Scanning Calorimetry (DSC) in a Perkin Elmer power compensation PE DSC7 apparatus.

Electrochemical characterization of anodes for Li ion batteries was performed by Galvanostatic Cycling (GC) tests carried out in polypropylene T cells using a lithium foil as counter electrode and fiber glass disks (Whatman R) soaked with the electrolyte as separators. Electrodes were prepared, from a slurry composed by bimetallic alloys, binder and electronic support (graphite), by a deposition as a thin film on a copper foil, employing the doctor-blade technique. The liquid electrolyte used was 1.0 M LiPF$_6$ in a 1:1 mixture of ethylene carbonate (EC) and dimethyl carbonate (DMC), Merck battery grade. GC tests were performed using a Maccor Series 4000 Battery Test System and an Arbin Instrument Testing System model BT-2000. The charge–discharge cycles were performed at various C rate regimes. A more detailed description of different experimental setups is reported in previous papers [13–15].
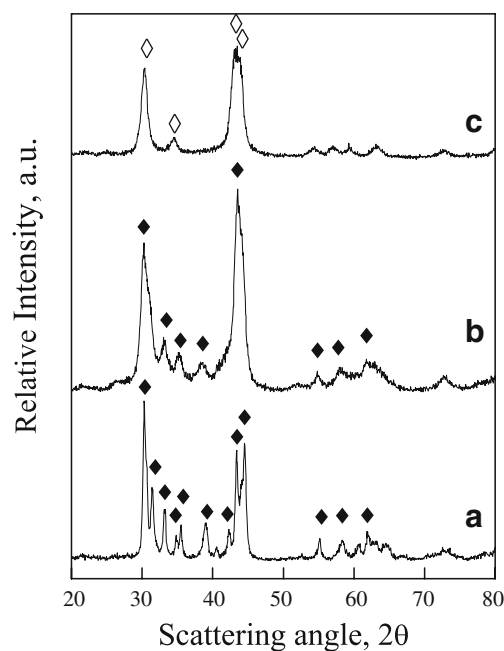
Fig. 1 Cu-Kα XRD patterns relevant to the as prepared Ni–Sn alloys: *a* Ni$_{38}$Sn$_{62}$; *b* Ni$_{44}$Sn$_{56}$; *c* Ni$_{58}$Sn$_{42}$. *filled diamond* Ni$_3$Sn$_4$, JCPDS 4-851; *empty diamond* Ni$_3$Sn$_2$ JCPDS 7-256

Results and discussion

Three nickel–tin mixtures of nominal compositions Ni$_{38}$Sn$_{62}$, Ni$_{44}$Sn$_{56}$, Ni$_{58}$Sn$_{42}$, were prepared by mechanical alloying starting from pure elements. The process resulted in the formation of nanostructured intermetallic phases whose XRD patterns are shown in Fig. 1. Structural and microstructural features of the milled powders are collected in Table 1.

According to the equilibrium binary phase diagram, the two mixtures of atomic composition Ni$_{44}$Sn$_{56}$ and Ni$_{38}$Sn$_{62}$, patterns a and b in Fig. 1, formed the monoclinic Ni$_3$Sn$_4$ intermetallic phase. While the content of microstrain was similar, the Ni$_{44}$Sn$_{56}$ showed smaller average crystallite sizes. Conversely the tin content in the Ni$_{38}$Sn$_{62}$, in excess with respect to the intermetallic stoichiometry, probably hindered the microstructural refinement during mechanical processing, so limiting the diffraction domain size reduction even for longer milling times. The existence of a tin fraction not alloyed in this latter sample was confirmed by the presence of an endothermal peak in the DSC trace at 493 K, not reported here, corresponding to the melting temperature of elemental tin. Accordingly, the Bragg peaks relevant to the Sn tetragonal phase were observed in the XRD pattern of the annealed sample—see pattern a in Fig. 2.

Milling of the Ni$_{58}$Sn$_{42}$ mixture yielded a nanostructured Ni$_3$Sn$_2$ hexagonal phase, still in agreement with the binary phase diagram. The average value, <L>, of crystallite size ranged around 120 (±10) Å, with again about 0.5% of

Table 1 Microstructural features of the materials prepared by ball milling as evaluated by Rietveld refinement analysis

Atomic % composition of starting mixture	Milling time, h	Relative abundance wt.%	Crystallite average size, $<L>$, Å	Crystallite microstrain	Cell parameter Å
$Ni_{38}Sn_{62}$	70	Ni_3Sn_4 100 wt.%	344	1.5×10^{-3}	a=12.28 b=4.05 c=5.20 β=104.7
$Ni_{44}Sn_{56}$	50	Ni_3Sn_4 100 wt.%	151	5.6×10^{-3}	a=12.46 b=4.10 c=5.21 β=103.9
$Ni_{58}Sn_{42}$	64	Ni_3Sn_2 100 wt.%	120	5.3×10^{-3}	a=4.12 c=5.19
$Sn_{31}Co_{28}C_{41}$	58	CoSn 85 wt.% $CoSn_2$ 15 wt.%	CoSn 160 $CoSn_2$ 90	1.8×10^{-4} 6.3×10^{-4}	a=5.29 c=4.26 a=6.37 c=5.44
$Sn_{31}Co_{28}C_{41}$	72	CoSn 100 wt.%	140	8.9×10^{-5}	a=5.30 c=4.26
$Sn_{31}Co_{28}C_{41}$	102	CoSn 100 wt.%	124	1.5×10^{-3}	a=5.31 c=4.26

microstrain level. Broad exothermal signals characterised the DSC curves of the $Ni_{44}Sn_{56}$ and $Ni_{58}Sn_{42}$ alloys, ascribable to grain growth of the equilibrium intermetallic phases, as it is observable in XRD patterns b and c of Fig. 2, relevant to the annealed samples.

As representative measurements of electrochemical activity of these materials, in Fig. 3 we report the room temperature specific capacity during cycling tests, performed at different C-rates (from C/10 to 1C). To be noticed, all the curves showed good capacity retention and a satisfactory cycling efficiency of about 99%. The results of the most recent durability tests, with hundreds of cycles, confirmed this statement. For all the samples, the specific capacity associated with the reversible cycles was about 40% less than that associated with the first discharge. This initial decay in capacity, as already discussed [16], is probably associated with both the formation of $Li_{4.4}Sn$ alloy and the solvent decomposition, with the formation of a passivation film on the electrode surface.

The cycle performance of $Ni_{44}Sn_{56}$ was the highest among the three samples, showing discharge capacity of about 250 mA h g^{-1} at C/10 rate and about 200 mA h g^{-1} at 1C after 50 cycles. The $Ni_{38}Sn_{62}$ and $Ni_{58}Sn_{42}$ samples showed similar cycle characteristics, but with lower specific capacity values, in particular, at high current densities. A unique feature observed in Fig. 3 is the increase in capacity with the number of cycles for the $Ni_{44}Sn_{56}$ electrode. As already assessed [17], this may be due to anode surface evolution accompanying volume changes during cycling, which should lower the resistance to the Li diffusion within the electrode.

The results of the electrochemical tests may be related to the structural characteristics presented above. In the nano-crystalline Ni_3Sn_4 the synergic and complementary action of Sn and Ni seemed to work better than in the active tin, poorer Ni_3Sn_2. The smaller grain size of Ni_3Sn_2, as measured in the $Ni_{58}Sn_{42}$ specimen, did not permit to overcome this detrimental effect. In $Ni_{38}Sn_{62}$, the Sn excess accompanying the Ni_3Sn_4 phase made the working electro-

chemical system biphasic, also reducing the fraction of intermetallics in the electrode. Such features, together with larger intermetallic average crystallite size, could explain its lower electrochemical performance compared to the $Ni_{44}Sn_{56}$ stoichiometry. This last sample turned out to be a single nanostructured phase corresponding right to the intermetallic composition.
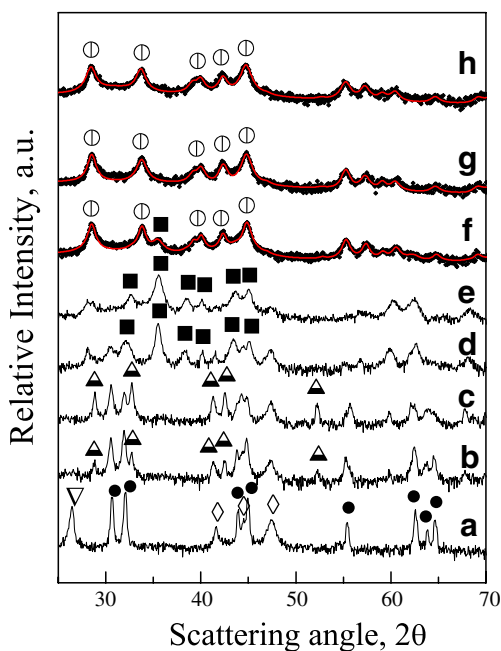
The other anode material we focus on here is the ternary Sn–Co–C system, in the at.% composition of $Sn_{31}Co_{28}C_{41}$. Recent works on composite anodic materials [21] evidenced a multifold action of C, well beyond the simple electrical support, especially for selected compositions. This prompted us to focus on that ternary system, including C in the starting milling mixture, and to prefer this stoichiometry. The mechanical treatment was effective in
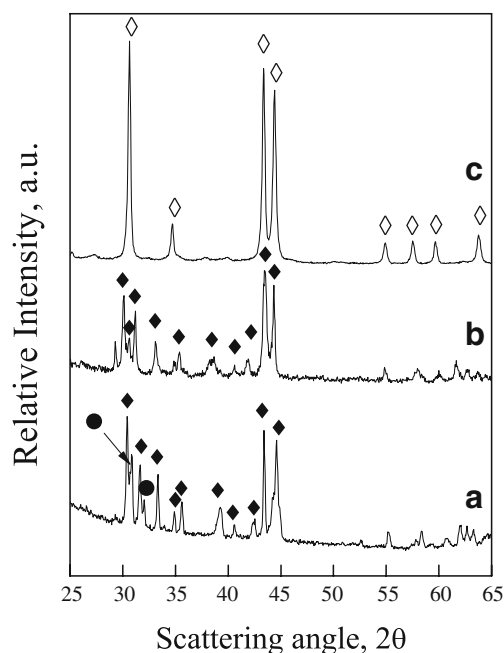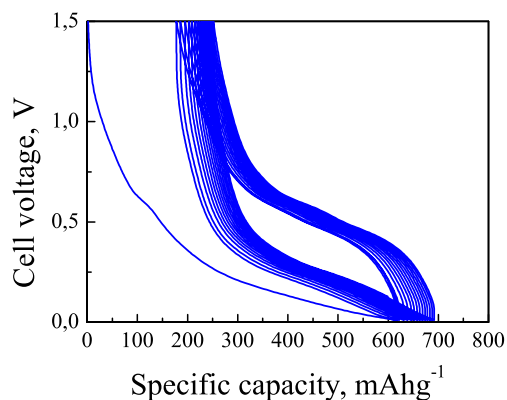

Fig. 2 Cu-Kα XRD patterns relevant to Ni–Sn alloys after DSC treatment up to 873 K. *a* $Ni_{38}Sn_{62}$; *b* $Ni_{44}Sn_{56}$; *c* $Ni_{58}Sn_{42}$. *filled diamond* Ni_3Sn_4, JCPDS 4-851; *empty diamond* Ni_3Sn_2 JCPDS 7-256; *filled circle* Sn JCPDS 4-673
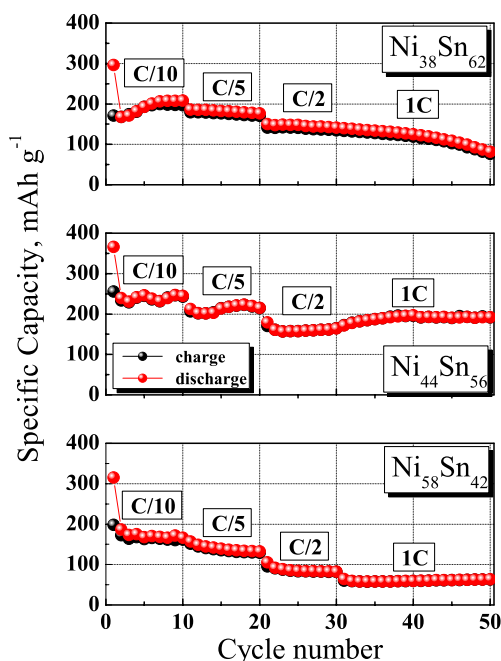
Fig. 3 Room temperature cycling performance of the three Ni–Sn alloy electrodes at C-rates ranging from C/10 to 1C, in the potential range of 0.02 to 1.20 V vs. Li/Li$^+$
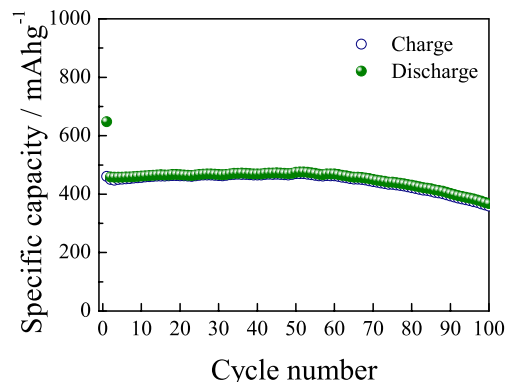

Fig. 5 Voltage vs. specific capacity profiles for the $Sn_{31}Co_{28}C_{41}$ 58 h milled sample based electrode at C/4 current rate and room temperature in a Li cell, voltage limits 0.01–1.5 V. 1C current rate was about 1.25 A cm^{-2} g^{-1}

obtaining a nanostructured single phase isomorphic to CoSn after a milling period of about 100 h in the present experimental conditions. The synthesis of such a phase did not occur as a direct alloying of the starting elements but through a more complex structural evolution which is described by the XRD patterns sequence reported in Fig. 4. The first effect of the mechanical treatment was the disappearance of the original C crystallinity, which, in the subsequent processing, seemed to act as a lubricant, coating metallic particles under treatment, but without reacting with them. After 8 h of milling Co and Sn habits are still present together with a further crystalline phase, not corresponding to any equilibrium intermetallics or carbides reported in the relevant phase diagrams. Its detailed identification is, at present, under study. Further mechanical processing induced the consumption of such phase and of residual pure elements to form a nanocrystalline CoSn$_2$ type structure. This latter was the only phase in the pattern relevant to the specimen subjected to 46 h of milling. Further mechanical treatment promoted the progressive transformation to CoSn, as observable in the upper patterns of Fig. 4, respectively,

Fig. 4 Cu-Kα XRD pattern sequence relevant to the structural evolution occurring during the processing of the $Sn_{31}Co_{28}C_{41}$ powder mixture. *a* 15 min of milling, *b* 8 h, *c* 16 h, *d* 32 h, *e* 46 h, *f* 58 h, *g* 72 h, *h* 102 h. For the longer treated specimens the Rietveld refinement profiles are also reported. *Empty inverted triangle* C (Graphite) JCPDS 12-212; *filled circle* Sn JCPDS 4-673; *empty diamond* cobalt JCPDS 5-727; ≅ unknown phase; *filled square* CoSn$_2$ JCPDS 25-256; 2 CoSn JCPDS 2-559

Fig. 6 Specific capacity plotted as a function of cycle number for $Sn_{31}Co_{28}C_{41}$ 58 h milled sample registered at C/4 rate and room temperature vs. Li/Li$^+$

72 and 102 h of milling. Microstructural details and relative abundance of Co–Sn phases, estimated by the Rietveld approach, are reported in Table 1. The electrochemical investigation was carried out over the 58, 72, and 102-h milled samples [13, 14], and in this paper we focus on the specimen treated for 58 h, in which both the intermetallic compounds were present.

As a representative electrochemical test, in Fig. 5, we report voltage versus specific capacity profiles measured during cycling in a lithium cell at C/4 current rate. Besides the tin–lithium alloying–dealloying process above described, a contribution of graphite, in reversibly hosting Li should be taken into account according to the reaction:

$$6C + Li \leftrightarrow LiC_6 \qquad (2)$$

[13, 14]. As expected, irreversible processes characterized the first cycle which can involve electrode structural evolution and formation of passivation layers, as well as electrolyte decomposition phenomena. Specific capacity from the first discharge can be evaluated as 647 mA h g^{-1}, then the subsequent cycles showed a high reversible specific capacity, about 450 mA h g^{-1}. This latter value is 49% of the theoretical one, as estimated on the base of the processes (1) and (2), representing the active part of $Sn_{31}Co_{28}C_{41}$ compound. As shown in Fig. 6, the cell is also quite stable over 100 cycles, the charge/discharge efficiency approaching 100%. Finally, this anodic material also evidenced a good structural stability: XRD analysis performed after the cycling test did not show any relevant variation. The electrochemical results are quite similar to what was observed for the sample milled 102 h and discussed in a previous paper [13]. The electrochemical role of the about 15 wt.% of $CoSn_2$ is, at present, the object of further deepening.

Conclusions

Even though quite recent, the interest in using mechanochemical techniques to prepare nanostructured electrode materials is continuously rising. Within this research field, the outcomes of the electrochemical tests of some of the studied systems appear to be of applicative value. Moreover, although the interpretation of the electrochemical behaviour on the basis of the structural characteristics is not immediate, a correlation between them emerges from the presented data. A further improvement in synthesis route and strategy could be reached by taking into account the specific milling dynamic parameters as well as evaluating proper impact energy and milling intensity values. It is right on this direction that our study is going further.

References

1. Aricò AS, Bruce P, Scrosati B, Tarascon JM, Van Schalkwijk W (2005) Nature Materials 4:366
2. Jiang C, Hosono E, Zhou H (2006) Nanotoday 1(4):28
3. Tarascon JM, Armand M (2001) Nature 414:359
4. Dell RM, Rand DAJ (2001) J Power Sources 100:2
5. Scrosati B (1995) Nature 373:557
6. Srinivasan S, Mosdale R, Stevens P, Yang C (1999) Annu Rev Energy Environ 24:281–328
7. Suryanarayana C (2001) Prog Mater Sci 46:1
8. Heinicke G (1984) Tribochemistry. Akademie-Verlag, Berlin
9. Tarascon JM, Morcrette M, Saisnt J, Aymard L, Janot R (2005) C. R. Chimie 8:17
10. Proceedings of IMLB (2006) J Power Sources in press
11. Proceedings of MH (2006) J Alloys Compd in press
12. Mulas G, Schiffini L, Cocco G (2004) J Mater Res 19(11):3279
13. Hassoun J, Mulas G, Panero S, Scrosati B (2007) Electrochem Commun 9:2075
14. Hassoun J, Panero S, Mulas G, Scrosati B (2007) J Power Sources 171:928
15. Gerbaldi C, Nair J, Bonatto Minella C, Meligrana G, Mulas G, Bodoardo S, Dongiovanni R, Penazzi N J Appl Electrochem in press
16. Amadei I, Panero S, Scrosati B, Cocco G, Schiffini L (2005) J Power Sources 143:227
17. Mukaibo H, Sumi T, Yokoshima T, Momma T, Osaka T (2003) Electrochem Solid-State Lett 6(10):A218
18. Hassoun J, Panero S, Reale P, Scrosati B (2006) Int J Electrochem Sci 1:110
19. Hassoun J, Panero S, Scrosati B (2006) J Power Sources 160:1336
20. Lutterotti L, Ceccato R, Dal Maschio R, Pagani E (1998) Mater Sci Forum 278–281:87
21. Dahn JR, Mar RE, Abouzeid A (2006) J Electrochem Soc A361:153